Supporting Information for
"Impact of spatially correlated pore-scale heterogeneity on drying porous media"

Oshri Borgman,[1] Paolo Fantinel,[2] Wieland Lühder,[2] Lucas Goehring[2,3], and Ran Holtzman[1]

[1]Department of Soil and Water Sciences, Hebrew University of Jerusalem, Rehovot, Israel,
[2]Max Planck Institute for Dynamics and Self-Organization, Göttingen, Germany,
[3]School of Science and Technology, Nottingham Trent University, Nottingham, UK

Introduction

This document includes (i) example of vapor saturation profiles showing the two-dimensional structures that develops in the boundary layer; (ii) the complete set of drying patterns (at breakthrough) and drying curves (rate vs. saturation) from all microfluidic experiments with corresponding simulations of similar pore geometry; and (iii) videos highlighting the dynamic evolution of the drying pattern in experiments and simulations.

(i) Vapor concentration profiles in the boundary layer

The atmospheric demand of vapor, which sets the potential rate of evaporation from the porous media, is controlled by vapor diffusion in the air boundary layer that forms above the medium's open surface. We extend here our model to include calculation of the vapor concentrations and fluxes in this layer, by discretizing it into a network of interconnected cells. This captures the coupling between the porous media and the boundary layer, namely the surface-wetness dependent distribution of vapor concentration. As a pore on the sample surface dries, the vapor flux through it decreases, enhancing the vapor flux of an adjacent wet pore due to a transverse (parallel to the surface) vapor diffusion (Fig. S1 [Shahraeeni et al., 2012].

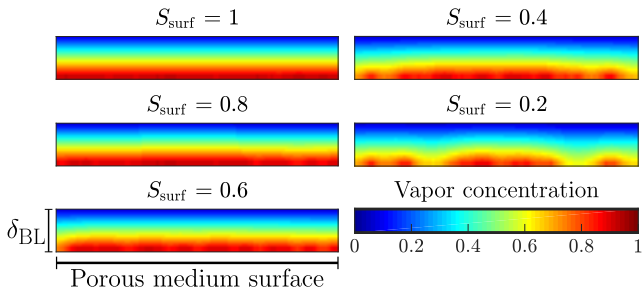

Figure S1. Vapor concentrations ϕ in the boundary layer above the surface of the sample during a simulation (surface saturation S_{surf} decreases in time). The gradual transition from a 1-D concentration profile for high S_{surf} to a 2-D profile at low S_{surf} is driven by enhanced transverse diffusion of vapor in the boundary layer. The location of the porous medium surface and the boundary layer (of width δ_{BL}) are indicated on the panel with S_{surf} = 0.6; porous medium not shown.

Corresponding author: Ran Holtzman, `holtzman.ran@mail.huji.ac.il`

(ii) Comparison of experiments and simulations

For completeness, we provide in Fig. S2 the entire set of drying patterns (at breakthrough) from all microfluidic experiments, alongside with the corresponding simulated patterns (for similar pore geometry), and the drying curves (rates vs. saturation) for both. We also provide the theoretical rates obtained by solving Laplace's equation (Eqs. 1–2 in the main text) for the pore-by-pore sequence of experimental patterns (Fig S3). Data shown here includes 8 experiments with no spatial correlation ($\zeta = 0$, Fig. S2) and 14 experiments with correlated porous media ($\zeta > 0$, Fig. S2 cotinued). The data set for ζ=0 includes four λ values, with two experimental realizations (different random pillar sizes) for each combination of ζ and λ (total of 8 different sample designs). For the correlated samples, data includes two disorder values (λ=0.1, 0.2) and four correlation values (ζ=1, 4, 10 and 15), again totaling 8 sample designs. For each pair of experimental and simulated patterns, we provide the match in patterns, at breakthrough. For each sample, we also provide the pore sizes (in terms of volume, normalized by the mean).

The experiments with ζ of 1 and 4, λ=0.1, and with ζ=15, λ=0.2, were repeated three times using samples with similar design (made from the same mold), albeit with small differences due to manufacturing errors. As these errors are small (~1.6 μm in pillar size, ~3.2% of design), the difference between emergent patterns demonstrates the sensitivity of the patterns to small details, where slight changes in pore sizes, even locally, can significantly alter the pattern. An extreme case of the this sensitivity is exemplified by the distinctively different patterns observed when repeating experiments with $\lambda = 0.2$, $\zeta = 15$ (using the same mold, i.e. same design). We believe that the reason lies in a "binary choice" occurring when the invasion front reaches a bottleneck (a narrow throat); when such a throat is slightly shrinked (due to manufacturing error), the invasion may proceed elsewhere, completely avoiding an entire region. The good match between the experimental rates and the theoretical rates obtained from the observed experimental patterns (Fig S3; with the exception of $\zeta = 0$ and $\lambda = 0.05$, and (ii) $\zeta = 10$ and $\lambda = 0.2$, see below), confirms the validity of our evaporation and vapor transport calculations. It further suggests that differences between our simulated and experimental rates can result from small manufacturing errors which alter the experimental patterns (see main text for further details).

Another variation within experiments is their initial drying rate, associated with differences in the designed width of the boundary layer δ_{BL} (2±1 mm), and its extension into the air just outside the cell. While in most experiments the initial rates are limited to a range of 0.1–0.3 μm/s, in two cases we observed exceptionally higher rates: (i) $\zeta = 0$ and $\lambda = 0.05$, and (ii) $\zeta = 10$ and $\lambda = 0.2$. The former experiment was repeated (using a different sample design), providing a similar rate (~0.5 and ~0.6 μm/s). The latter, which shows an unusual high rate (almost 1 μm/s), was not repeated. The disagreement between the measured rates (initial values as well as their evolution with time) and the theoretical values computed from the experimentally observed patterns of these 3 experiments (Fig S3), suggests that care must be taken in interpreting these experiments. Finally, we note the fluctuations in experimental rates, introduced by their evaluation from analysis of the time-lapse images. While taking great care to ensure constant environmental conditions, some additional noise may also be introduced by changes in the air circulation in the laboratory.

(iii) Videos showing dynamics of pattern evolution

Here, we compare the evolution of the experimental and simulated drying pattern via a pair of videos, Borgman-ms01 and Borgman-ms02, respectively (for $\zeta = 4$). The videos emphasize the main difference: isolated clusters in the simulations tend to dry out faster than in the experiments, as reflected in the evolution of Euler number. The disappearance of isolated liquid clusters reduces the wetness near the surface and advances the air-liquid interface deeper into the porous medium, resulting in a notable decrease in drying rates.

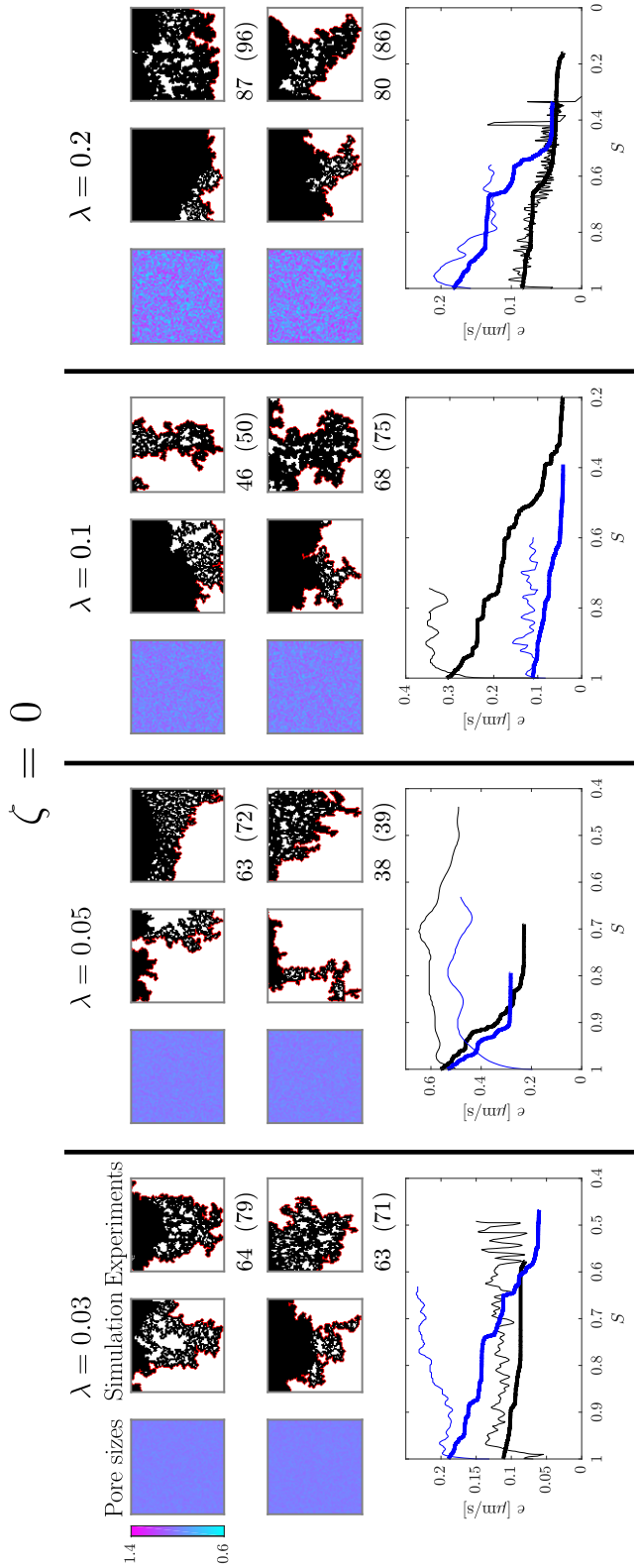

Figure S2. Pore size distribution, simulated and experimental drying patterns at breakthrough, and pattern match (in %, parentheses provide match considering only the leading front), for uncorrelated samples (ζ=0) of various heterogeneity (λ). In the patterns, black and white represent dry and wet pores (solid not shown); red line marks the invasion front. Experimental and simulated drying curves (rates vs. liquid saturation) are plotted in thin and thick lines, respectively. Black and blue lines correspond to the upper and lower sample (which has different random seed, same ζ and λ).

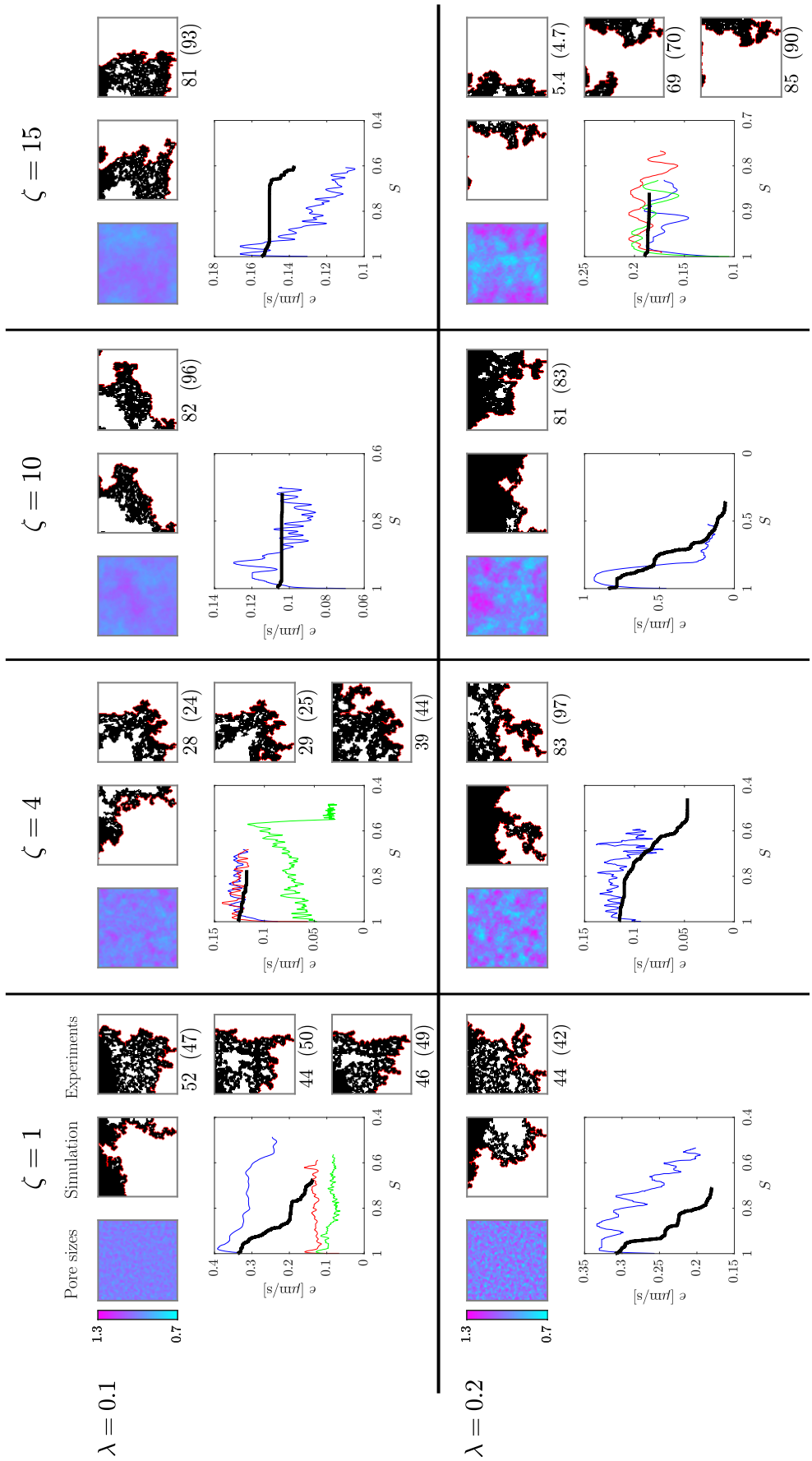

Figure S2. (continued) Pore size distribution, simulated and experimental drying patterns at breakthrough, and pattern match (in %, parentheses provide match considering only the leading front), for correlated samples (ζ= 1, 4, 10, and 15) and various λ. Black and white represent dry and wet pores (solid not shown); red line marks the invasion front. In cases where several experimental runs were made on the same sample design, blue, red and green *thin* lines show rates corresponding to the patterns of the upper, middle and lower experimental runs. Black thick line is the simulated rate, using an effective boundary layer evaluated from the upper experimental run.

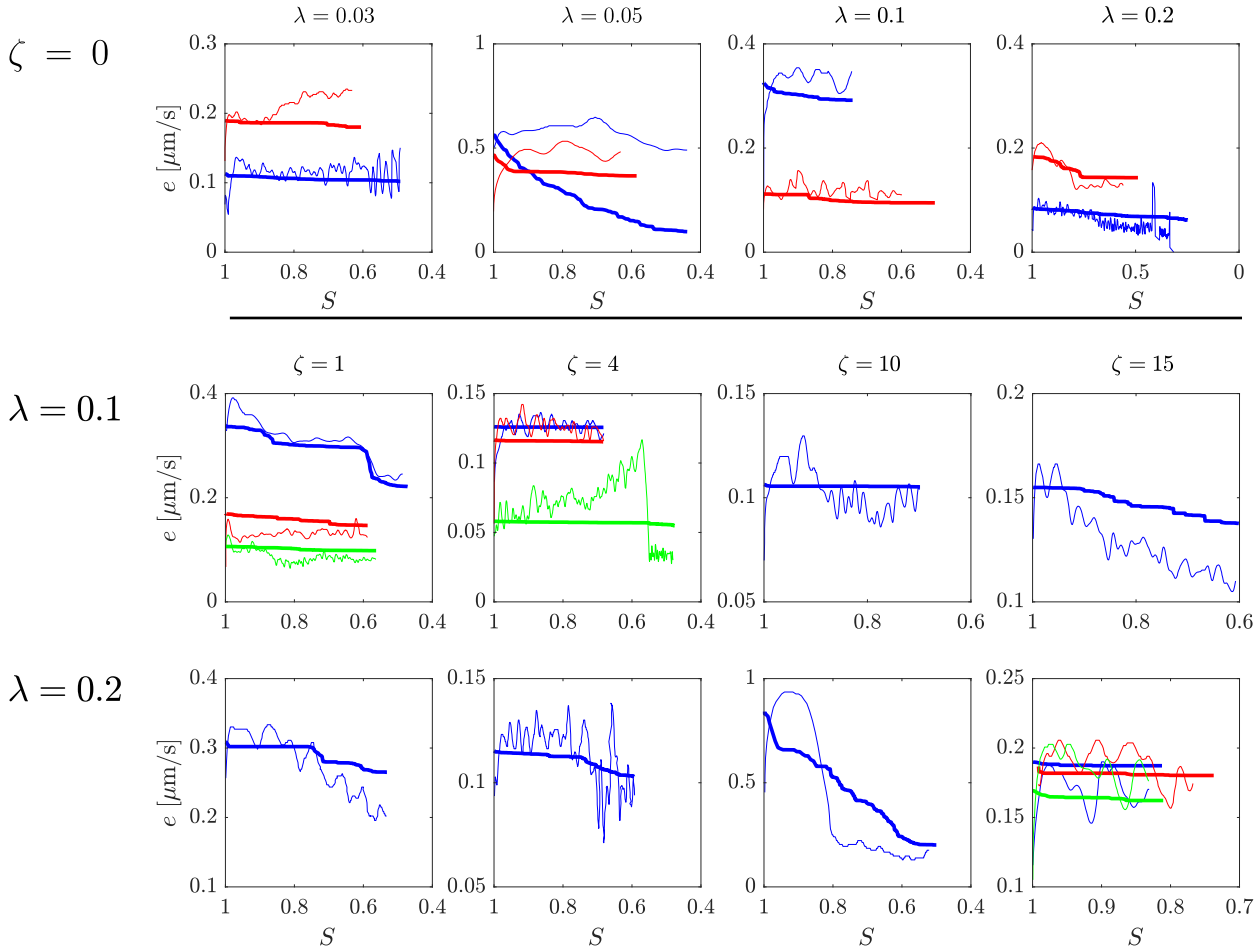

Figure S3. Comparison of experimental rates (thin lines) with the theoretical rates (thick lines) predicted by solving Laplace's equation for the pore-by-pore sequence of observed experimental patterns.